ภาควิชาวิศวกรรมเหมืองแร่และวัสดุ
คณะวิศวกรรมศาสตร์
มหาวิทยาลัยสงขลานครินทร์

การสอบปลายภาค ประจำภาคการศึกษาที่ 1 ปีการศึกษา 2558

วันที่ 15 ธันวาคม 2558 เวลา 09.00-12.00 น.

วิชา 237-407 Failure Mechanics and Analysis ห้อง A200

<u>คำชี้แจงสำหรับนักศึกษา</u>

1. ข้อสอบมีจำนวน 5 ข้อ จำนวน 4 หน้า รวมใบปะหน้านี้
2. เอกสารประกอบข้อสอบ Failure analysis of hydraulic turbine shaft และข้อมูลอื่นๆ ที่เกี่ยวข้อง รวม 14 หน้า
3. ตอบคำถามลงในสมุดคำตอบ เขียนหมายเลขข้อให้ชัดเจน
4. สามารถนำเอกสารทุกชนิด และอุปกรณ์ช่วยสอบได้ทุกชนิดเข้าห้องสอบได้
5. คะแนนสอบครั้งนี้คิดเป็น 30 % ของคะแนนรวมทั้งหมด

<u>คำชี้แจงสำหรับกรรมการจัดทำข้อสอบ และผู้คุมสอบ</u>

1. ให้แจกสมุดคำตอบคนละ 1 เล่ม

อ. ณรงค์ฤทธ์ โทธรัตน์
ผู้ออกข้อสอบ

ข้อที่	คะแนนเต็ม	คะแนนของนักศึกษา
1	15	
2	20	
3	15	
4	20	
5	30	
คะแนนรวม	100	

แบบทดสอบการวิเคราะห์การชำรุดอย่างเป็นระบบ ปีการศึกษา 2558

I. ข้อกำหนดในการสอบ

1. สามารถนำเอกสารทุกชนิด และอุปกรณ์ช่วยสอบได้ทุกชนิด เข้าห้องสอบได้

2. จากรายงานผลการวิเคราะห์การชำรุด 1 ฉบับ

Case Study : *Failure Analysis of Hydraulic Turbine Shaft*

ให้นักศึกษา ใช้ความรู้ ด้าน Fracture Mechanics, Systematic Failure Analysis, Heat Treatment, Metallurgy, Materials Engineering, Manufacturing Process และความรู้อื่น ๆ ด้านวิศวกรรมศาสตร์ อธิบายผลการวิเคราะห์เพื่อใช้ในการตอบข้อสอบ

3. เวลา 3 ชั่วโมง ข้อสอบมีทั้งหมด 4 กลุ่มเป้าหมาย (Materials Analysis, Process Analysis, Failure Analysis, Management & Prevention)

II. วัตถุประสงค์ในการสอบ

เพื่อให้นักศึกษาสามารถวิเคราะห์ปัญหาทั้งระบบ นำทฤษฎี มาเชื่อมโยงกับการปฏิบัติ และประยุกต์ใช้ในการอธิบายปรากฏการณ์ที่เกิดขึ้นกับชิ้นงานจริงและมองในเชิงการบริหารและจัดการทางวิศวกรรมได้

เหตุการณ์สำคัญ

โรงไฟฟ้าพลังน้ำของประเทศ Serbia ถูกออกแบบให้ติดตั้ง Hydro Turbine แบบ KAPLAN ขนาดเครื่องละ 28 MW จำนวน 9 ชุด

Turbine 3 ชุด แรก อายุ 20 ปี

Turbine 3 ชุด ที่ 2 อายุ 15 ปี

Turbine 3 ชุด ที่ 3 อายุ 10 ปี

กำหนดอายุใช้งาน Shaft ที่ 30 ปี (200,000 ชม.) และจะมีการ Renovate (ปรับปรุงระบบ) ทั้ง ชุด Turbine, Shaft และ Generator ของ Turbine 3 ชุด แรก

หลังจากเดินเครื่องได้ 163,411 ชม. (20 ปี) พบ Turbine 1 ตัว ของชุดแรก น้ำมันหล่อลื่นของ Runner Servomotor รั่วออกจาก Chamber และมีการวิเคราะห์การชำรุดตามรายงาน

ผู้ออกข้อสอบ : ณรงค์ฤทธ์ โทธรัตน์

ให้นักศึกษาตอบคำถามดังต่อไปนี้

1. ในรายงาน ในหัวข้อ Introduction บรรยายว่า โดยปกติทั่วไป ปัญหาของ โรงไฟฟ้าพลังน้ำ พบอาการชำรุดแบบ Erosion และ Cavitation แต่ถ้าหากพบว่าเกิดชำรุด แบบ Corrosion, Erosion และ Cavitation ให้นักศึกษาอธิบาย ความแตกต่างระหว่างการชำรุดทั้ง 3 รูปแบบ (15 คะแนน)

2. Root cause ของการชำรุด ของ Turbine Shaft จากการสรุปของรายงาน คือ สาเหตุใด อธิบายกลไกการชำรุดเป็นขั้นตอนจนกระทั่ง Shaft มีการขยายตัวจนมีการตรวจพบของเหตุการณ์ครั้งนี้ ด้วยความรู้ด้าน Fracture Mechanics และ Failure Analysis ขนาดของภาระเป็นสาเหตุหลักของการชำรุดหรือไม่ เพราะเหตุใด (20 คะแนน)

3. หากนักศึกษาเป็นวิศวกรของโรงไฟฟ้านี้ จะดำเนินการบริหารจัดอย่างไรกับ Shaft ที่กำลังใช้งานอีก 8 ตัว และจะป้องกันได้อย่างไรกับ Shaft ที่ยังไม่พบการแตกร้าว (15 คะแนน)

4. วิจารณ์ การเลือกใช้วัสดุ การเลือกใช้กระบวนการผลิต และกระบวนการ Heat Treatment ในการผลิต Shaft และ Flange ชุดนี้ มีข้อดีและด้อยอย่างไร กระบวนมีผลต่อคุณสมบัติทางกลและทางโลหะวิทยาเป็นอย่างไร มีผลต่อโอกาสเกิดการชำรุดอย่างไร (20 คะแนน)

5. ถ้าหากนักศึกษาเป็นวิศกรวัสดุผู้ได้รับมอบหมายให้รับผิดชอบโครงการที่จะ Renovate ชุด Turbine ตัวที่ชำรุดและอีก 8 ชุดที่เหลือ จะมีวิธีการบริหารจัดการอย่างไรบ้าง (30 คะแนน)

ผู้ออกข้อสอบ : ณรงค์ฤทธ์ โทธรัตน์

เอกสารประกอบการสอบ 2558

Kaplan Type Hydro-power Plant

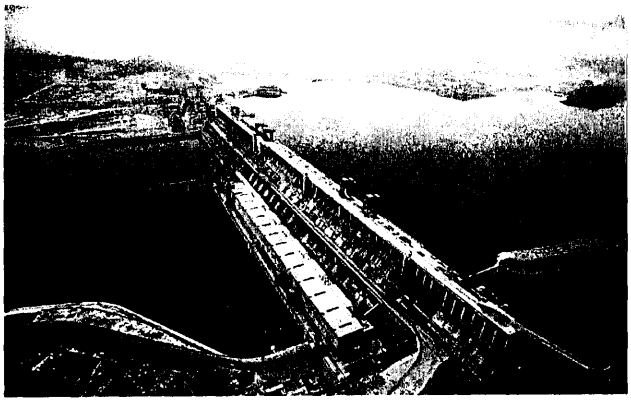

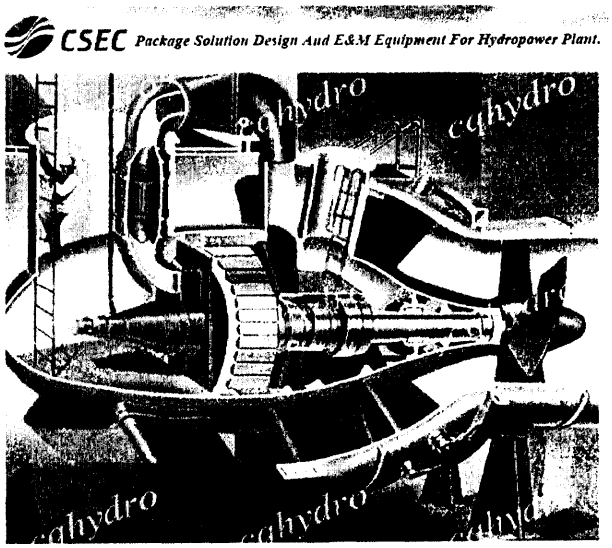

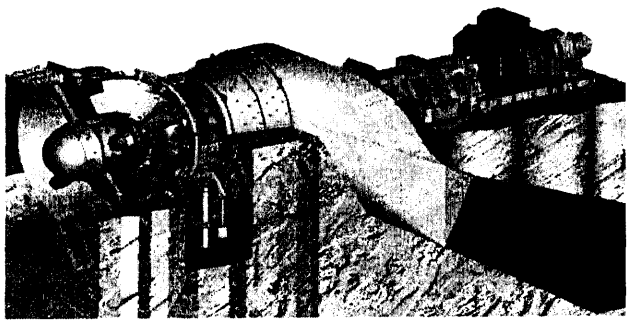

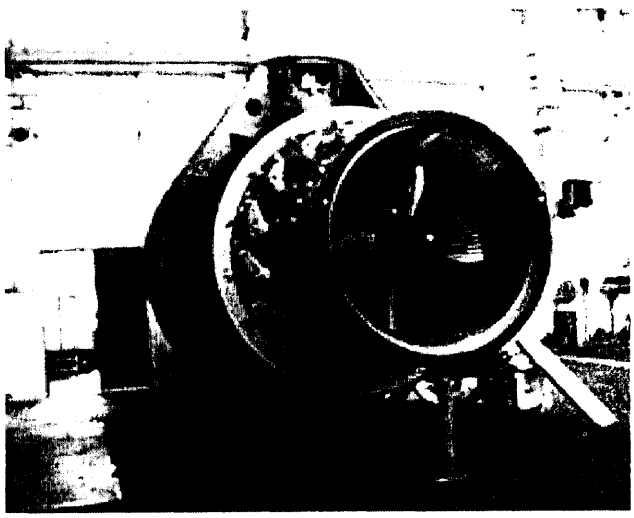

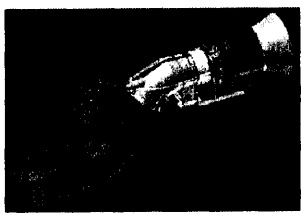

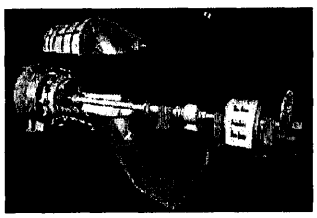

Engineering Failure Analysis 20 (2012) 54–66

Contents lists available at SciVerse ScienceDirect

Engineering Failure Analysis

journal homepage: www.elsevier.com/locate/engfailanal

Failure analysis of hydraulic turbine shaft

Dejan Momčilović [a], Zoran Odanović [a], Radivoje Mitrović [b], Ivana Atanasovska [c,*], Tomaž Vuherer [d]

[a] Institute for Testing of Materials IMS, Bulevar Vojvode Mišića 43, 11000 Belgrade, Serbia
[b] Faculty of Mechanical Engineering, University of Belgrade, Kraljice Marije 16, 11120 Belgrade, Serbia
[c] Institute Kirilo Savić a.d., Vojvode Stepe 51, 11010 Belgrade, Serbia
[d] Faculty of Mechanical Engineering, University of Maribor, Smetanova Ulica 17, 2000 Maribor, Slovenia

ARTICLE INFO

Article history:
Received 26 April 2011
Received in revised form 29 September 2011
Accepted 18 October 2011
Available online 24 October 2011

Keywords:
Failure analysis
Shafts
Cracks
Corrosion fatigue

ABSTRACT

This paper describes the analysis of major failure of 28 MW horizontal hydro turbine shaft. The analysis of load carrying capacity of critical radius and fractography analysis are presented. Special emphasize is on metallurgical failure analysis of in-service crack initiation. The analysis of stresses is obtained by the finite element method and the developed model and load conditions are described. Finite element analysis is performed for case of normal service and start-up regime.

Based on the failure analysis and numerical calculations, it could be concluded that the seal box design led to constant flow of river water in zone of critical radius which resulted as occurrence of corrosion fatigue cracks and major failure of turbine shaft. Suggestions for problem solution for the turbine shaft are also presented.

1. Introduction

Information about cracks and failures of rotor shafts is generally kept confidential by the plant management and by the machine manufacturer; therefore not all the cases have been reported and analyzed in literature, especially in the recent years [1]. Catastrophic failures in hydro-power plants are rare, mainly due to the fact that main problems during operation are related to cavitations, erosion and material defects. Serious problems are mainly expected on high head hydro-power plants having high water fall exceeding 250 m, caused by high water pressures, pressure variations and high water speeds [2–4]. Moreover, adequate preventive maintenance and clearly defined overhaul procedures in hydro-power plants significantly reduce failure occurrences [5].

This paper describes the failure analysis of turbine shaft Kaplan's 28 MW bulb turbine. The bulb turbine generator's horizontal shaft, Fig. 1, is made by joining the forged and cast parts by slag welding, Fig. 2. The shaft is manufactured as hollow, housing a servomotor inside it, for shifting the runner blades. The flange, on which the crack occurred, is made of steel casting of 20GSL designation, according to GOST 977-88 [6]. The operating speed of turbine shaft was 62.5 rpm.

After in-service of 163,411 h, sudden oil loss was observed from the control system. Total projected operating life for the subject shaft is 200,000 h. Upon stopping the turbine and after visual inspection of all the spots where loss could have occurred a through-thickness crack was discovered of 2100 mm length, through which the turbine oil leaked from the runner servomotor chamber, Fig. 3. The residues of the anticorrosive coating and oil were detected as well as significant number of corrosion pits in the shaft-flange transition zone radius, Fig. 4. The location of this crack was on the flange radius, from the

* Corresponding author. Tel.: +381 63 362 957; fax: +381 11 2439 851.
E-mail addresses: dejanmomcilovic@yahoo.com (D. Momčilović), rmitrovic@mas.bg.ac.rs (R. Mitrović), iviatanasov@yahoo.com (I. Atanasovska).

1350-6307/$ - see front matter © 2011 Elsevier Ltd. All rights reserved.
doi:10.1016/j.engfailanal.2011.10.006

Nomenclature

C	parameter of Paris-Erdogan equation (–)
F_a	axial hydraulic force (N)
F_p	axial force from pressure in servomotor (N)
M	parameter of Paris-Erdogan equation (–)
M_t	torque on the runner (Nm)
Q	pressure in servomotor
R	servomotor cylinder radius (m); stress ratio (–)
R	servomotor toggle radius (m)
S_{FL}	fatigue limit (MPa)
x, y, z	axes of cartesian coordinate system
ΔK_{TH}	threshold stress intensity, (MPa$\sqrt{}$m)
σ_a	amplitude value of total normal stress (Pa)
σ_{eqv}	equivalent stresses calculated according to the Von Mises's criterion (Pa)
σ_n	total normal stress (Pa)
σ_{sr}	mean value of total normal stress (Pa)
σ_x	normal stress in direction of x axis (Pa)
σ_y	normal stress in direction of y axis (Pa)

cylindrical part of shaft towards the flange to which the runner is connected. After the failure, the shaft was disassembled and flame cut for the inspecting the fracture surface, Fig. 5.

2. Experimental results

2.1. Visual examination

On the basis of visual examination of the crack surface, the multiple fatigue cracks initiations sites were perceived, as shown in Fig. 6, (zone a). In the same figure, the zone of the stable fatigue crack propagation front, (zone b), and the final phase of instable crack growth are observed. In Fig. 6, (zone c), openings were perceived that had been drilled by mistake in some phase of the flange manufacture. The Fig. 7a and b shows the magnified view of the crack surface zones. Fig. 7a shows front view of fractured surface where are quite obvious ratchet marks that occurred as the result of linking the propagation fronts of several fatigue cracks, as well as the stable growth zone. Fig. 7b shows side view of shaft radius with secondary cracks. On the fracture surface, the visible distorted fatigue lines around numerous gas holes and locations of increased porosity are observed, Fig. 8.

The overall appearance of the examined crack surface indicates that the fracture occurred due to combined actions of twisting and bending. The small slant angle of the fatigue surface points to the influence of torsion stresses on cracks formation was less influential than the effects of the stress due to bending or tension. It can be seen in Figs. 5 and 6 that the through crack makes almost 30% of the total cross section of the shaft, so it is obvious that operating stresses in the fracture zone were small [7].

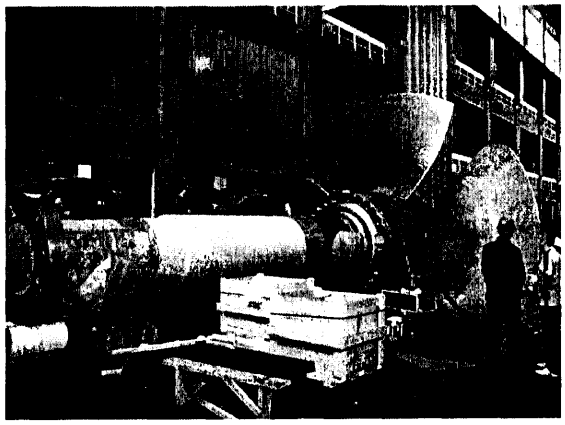

Fig. 1. Disassembled turbine shaft with runner.

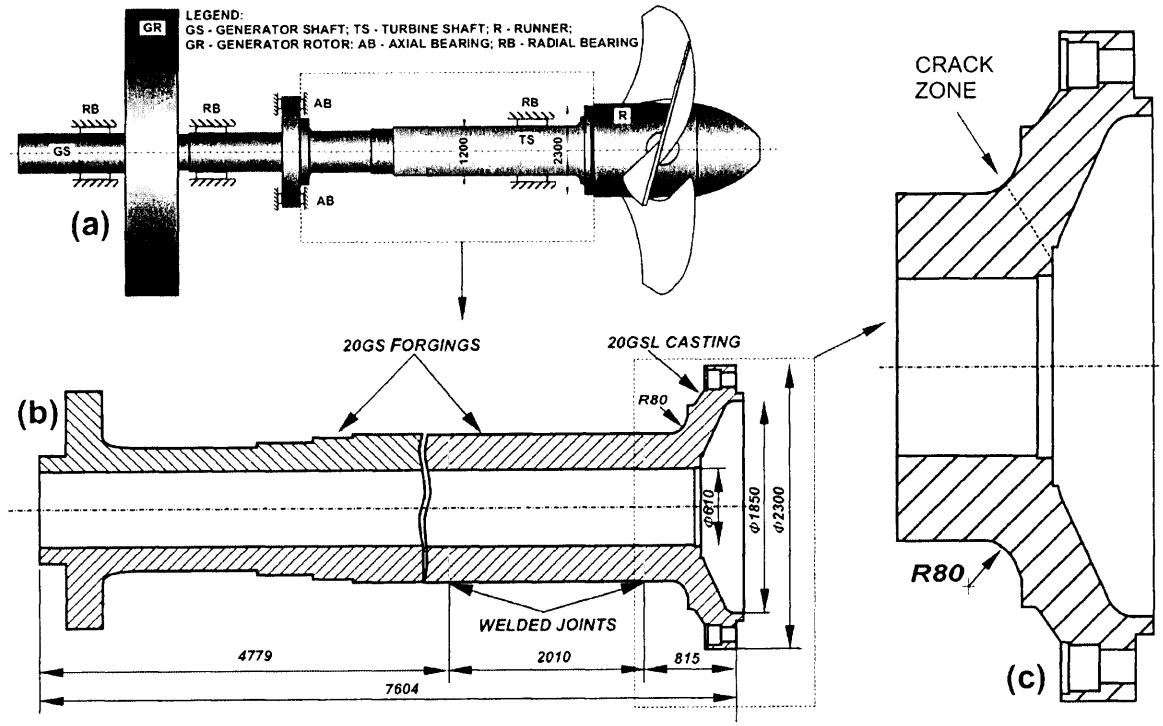

Fig. 2. Position of crack on general assembly of hydraulic turbine shaft: (a) schematic presentation of generator, (b) longitudinal cross section of the hollow shaft, and (c) longitudinal cross section of flange with crack detection zone.

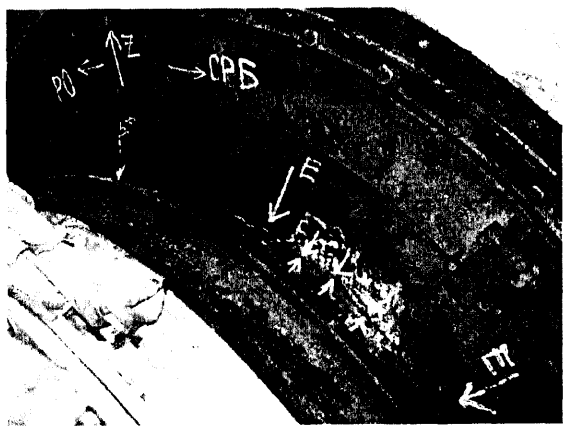

Fig. 3. General appearance of the cracked zone.

During cutting of samples for the mechanical and metallographic tests, numerous gas holes and pores were detected that resulted from the casting process, Fig. 9. Gas pores and holes were not perceived around the crack initiation location, i.e. around the outer shaft surface, but exclusively in the casting volume.

2.2. Chemical composition

Table 1 shows the chemical composition of flange material in accordance with the requirements of the reference standard [6]. The testing determined that the chemical composition meets this standard's requirements.

2.3. Mechanical properties

For the purpose of comparability of the testing results with the reference standard values [6], the tensile test was performed in conformity with the GOST 1497-84 standard requirements [8]. The test results are shown in Table 2. The samples were cut out from a casting, in direction parallel to the main shaft axis. Tensile specimens (15 specimens) were made

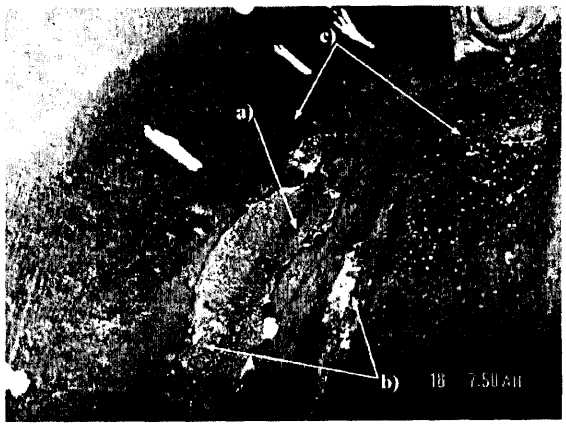

Fig. 4. Close view of the transient flange radius after detecting the crack: (a) main crack, (b) anti-corrosive protection layer, and (c) oil residue on corrosion pits.

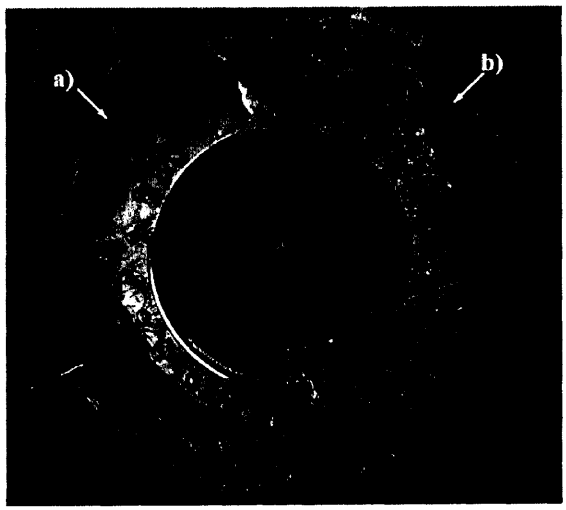

Fig. 5. Transversal cross section of the hollow shaft: (a) fractured zone of through wall crack on the hollow shaft and (b) flame cut zone of the shaft.

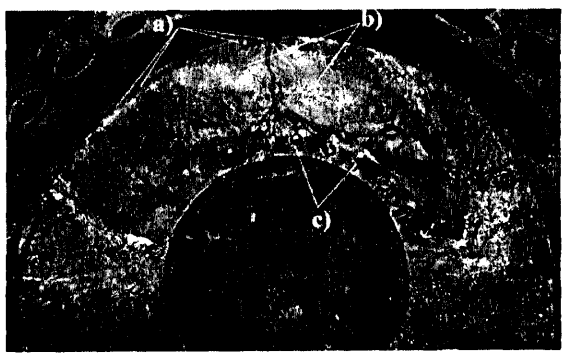

Fig. 6. General appearance of fractured surface: (a) multiple fatigue cracks initiations sites, (b) stable fatigue crack propagation front, and (c) drilled holes.

with larger cross section (with diameter of 20 mm), which enabled obtaining more reliable test results. The zone of cutting out of all samples for the mechanical and metallographic tests was 20 mm below to the external shaft surface.

Test-samples for impact (Charpy) toughness (25 specimens) are made as type 1, in compliance with the GOST 9454-78 [9], of the size 10 × 10 × 55 mm, with the U notch of 2 mm depth and with the 1 mm radius on top of the notch. The tests were made on instrumented Charpy pendulum and the obtained results show that in all the tested specimens, major fracture energy (90%) was used for crack initiation while its minor portion (10%) was spent on the crack propagation. The all values of

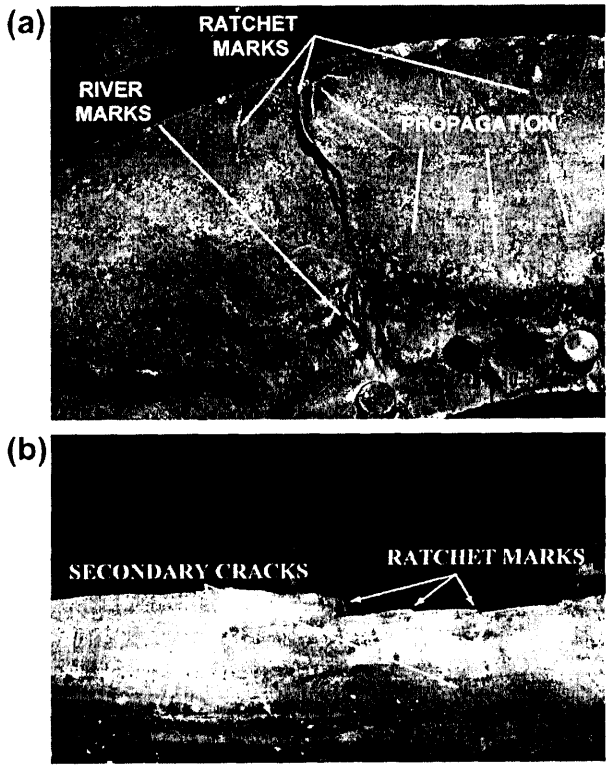

Fig. 7. Multiple crack initiation sites with ratchet marks: (a) front view and (b) side view.

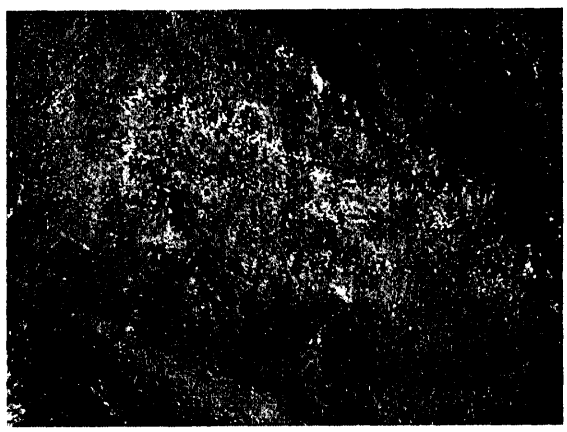

Fig. 8. Distorted fatigue beach marks on gas holes and porosity.

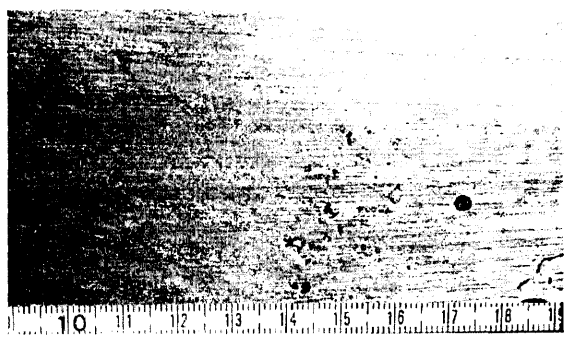

Fig. 9. Gas holes and shrinkages on casting, zone near shaft-flange transition radius.

Table 1
Chemical composition of flange material.

	%C	%Si	%Mn	%S	%P
Min	0.16	0.60	1.00		
Max	0.22	0.80	1.30	0030	0030

Table 2
Average and required mechanical properties at room temperature of the 20GSL steel casting [6].

	Average values	Standard deviation	Required (GOST 977) – min. values
Yield strength (MPa)	310	15.7	294
Tensile strength (MPa)	509	67.1	540
Elongation, in 2 in. (%)	17.6	7.3	18
Reduction of area (%)	35.2	13.2	30
Brinell hardness HB	153	7.4	–
Charpy-V notch, +20 °C (J)	74.4	36.3	23.4

impact toughness were above the minimal required values of 23.4 J (on + 20 °C according to GOST 977-88 [6]). The scatter of all results in all mechanical tests was observed, indicating the non-homogenous cast material microstructure.

2.4. Metallographic inspection

By reviewing the original documentation from the time of delivering and installing of the shaft, it was discovered that heat treatment of the shaft was done by applying the regime shown of Fig. 10:

Such a heat treatment regime indicates that complete austenization was done, with complete breaking of the microstructure that had remained from the casting process.

However, the microstructure of the material is the cast ferrite-pearlite one, with oxide type non-metallic inclusions and with minimal participation of dendrite structure, Fig. 11a. Dendrite structure presence points to the possibility of incomplete or irregularly executed shaft flange heat treatment, which explains the observed scatter of results in all the mechanical tests. It was also determined that there were large non-metallic oxide inclusions in the structure, which occurred in sequences. The fine microcracks were found in microstructure, Fig. 11b.

2.5. Fatigue properties

Testing of the fatigue strength was completed according to the requirements of the GOST 25.502/79 [10] standard, in open-air conditions, at the +20 °C, at load ratio $R = -1$. Fatigue limit S_{FL} of the shaft flange material was tested on ZWICK ROELL HB 250 and it is 168.0 MPa. The testing of fatigue crack growth with load ratio $R = 0$ was done at pulsator CRACTRONIC 160 on three specimens with the dimensions of cross section 12 × 22 mm. The results of fatigue tests are shown on Table 3.

2.6. Conclusion concerning the experimental results

Concerning the mechanical properties of the material, slight discrepancies were detected between the experimental results and the requirement of the specification [6]. Despite the fact that the results of tensile strength and elongation does not met the requirements this cannot be considered as significant for the failure of turbine shaft. Fatigue limit S_{FL} of flange material (168 MPa) is approx. 25% less then required (225 MPa) according to reference values, and could be indicated as significant factor to the premature failure.

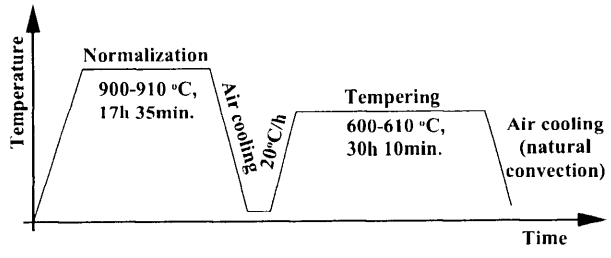

Fig. 10. Regime of applied heat treatment.

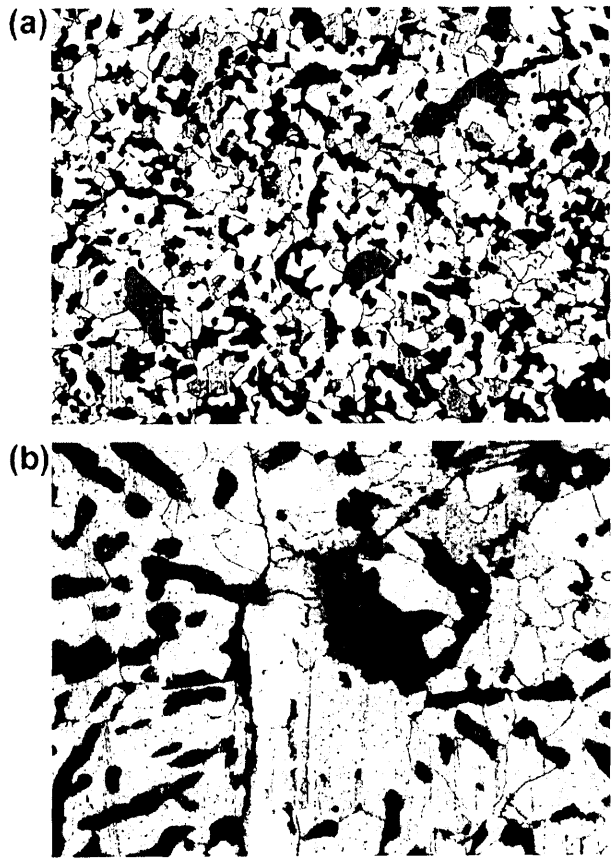

Fig. 11. Microstructure of flange material: (a). Cast, ferrite-pearlite microstructure, ×200, 5% nital, and (b). Microcracks emanating from shrinkage, ×500, 5% nital.

Table 3
Average and reference fatigue values of the 20GSL flange steel casting [11].

		Average values	Reference values	
Fatigue limit S_{FL} (MPa)		168[a]	On air 225	In water 140
Threshold stress intensity, ΔK_{TH} (MPa$\sqrt{}$m)		4.2[b]	–	
Parameters of Paris-Erdogan equation:	C	2.448×10^{-12}	–	
	m	3.584	–	

[a] Standard deviation for nine specimens that did not fail during test at 2×10^6 is 7.8 MPa.
[b] Standard deviation for three specimens threshold value is 0.3 MPa$\sqrt{}$m.

The presence of dendrite structure points to incomplete or irregular flange heat treatment. Moreover, microstructure and subsequent data scatter indicated that the heat treatment regime had some influence in the fracture process.

3. Numerical calculations

The linear Finite Elements Analysis is used for determining the stress state of turbine shaft and shaft flange attachment towards the turbine runner. The commercial ANSYS 11 software was chosen for finite element modeling. The shaft and flange dimensions have been defined by the turbine manufacturer in the original documentation, Fig. 2. The modeled 3D shaft-flange model is shown in Fig. 12.

3.1. Finite element model

Fig. 13 shows the finite element model of the analyzed shaft with flanges. The model represents a continuum discretized by the three-dimensional 8-node finite elements, with three degrees of freedom in each node (movement in the direction of x, y and z axes of the nodal coordinate system). The obtained model of regular finite elements mesh comprises 59420 nodes and 47547 elements and it enables simple following and reading of the stress state on critical radius circumference on radius

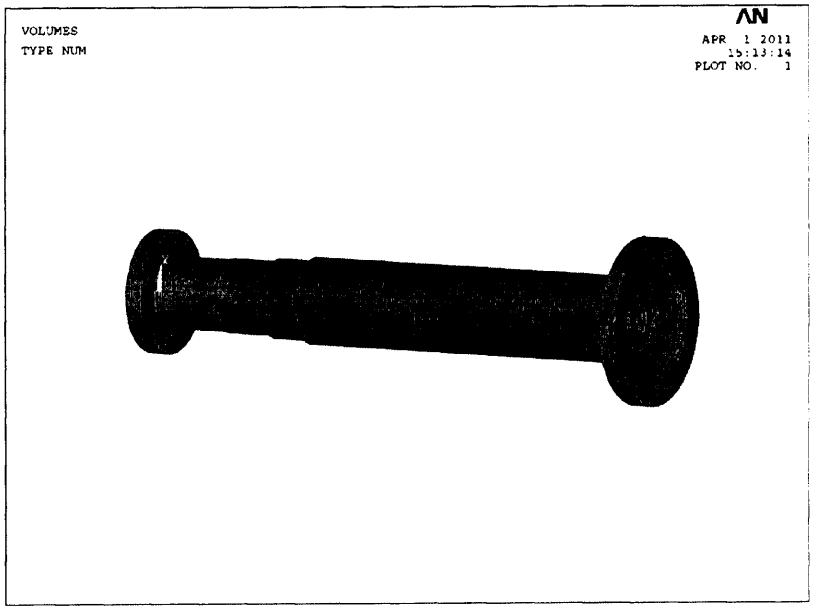

Fig. 12. 3D shaft model.

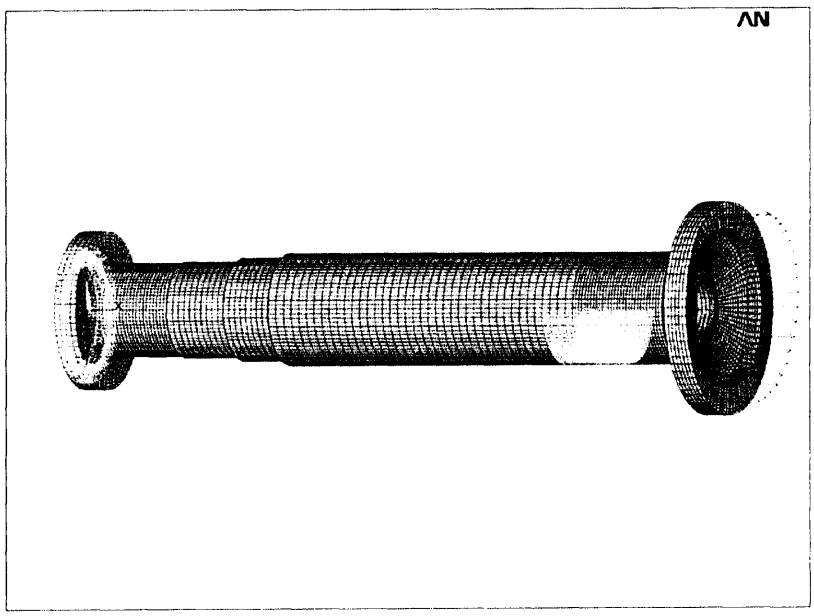

Fig. 13. Finite element model with defined boundary conditions and external loads for the load case 1.

flange. For modeling the elements to which the shaft is connected (generator shaft and turbine runner), boundary conditions have been defined on the model, as shown in Fig. 13: radial movements in the nodes in contact with sliding radial bearing and all movements at the flange attachment towards generator shaft.

3.2. External loads

Numerical calculation of the shaft-flange stress states was performed for two characteristic load cases. (The loads were taken from the original shaft manufacturer's documentation.)

Load case 1, Fig. 13, corresponds to the static load during start up regime of operation with the shift of the runner blades and it is defined by: the maximum axial hydraulic force of $F_a = 5542.65 \times 10^3$ N, pressure in servomotor of $q = 40$ bar, own shaft's weight, runner's weight of $1 \cdot 10^6$ N and the torque on the runner of $M_t = 4280.5935 \times 10^3$ Nm.

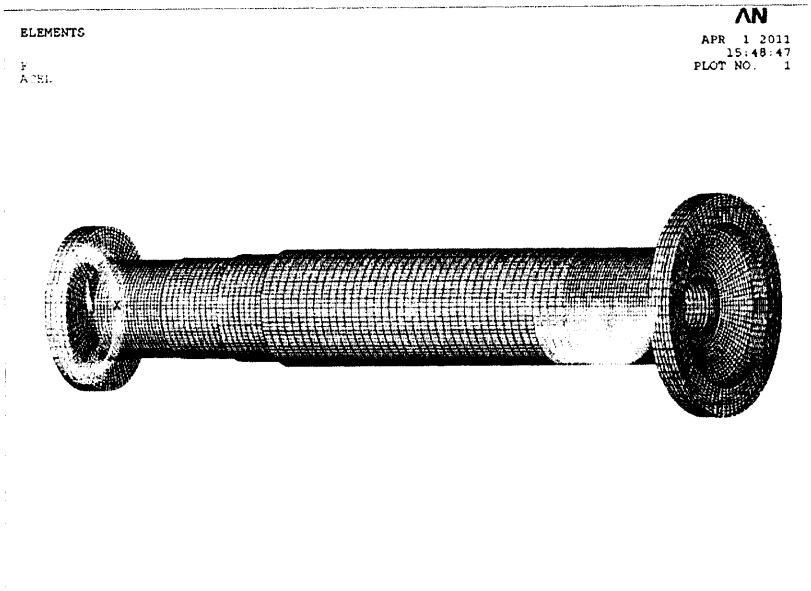

Fig. 14. Finite element model with defined boundary conditions and external loads for the load case 2.

Load case 2, Fig. 14, corresponds to the dynamic, time-variable load in the course of normal operating regime and it is defined by: axial hydraulic force of $F_a = 392.4 \times 10^3$ N, own shaft's weight, runner's weight of 1×10^6 N and the torque on the runner of $M_t = 4280.5935 \times 10^3$ Nm.

Figs. 13 and 14 shows the way of defining external loads and boundary conditions. The total axial hydraulic force F_a is simulated by the forces in axial direction (the x axis direction) at points of the shaft flange connection with the runner. The pressure in servomotor is simulated by surface pressure inside of flange and the axial force $F_p = p\ (R^2 - r^2)$, where the values of servomotor cylinder radius $R = 1.85/2$ m and servomotor toggle radius $r = 0.38/2$ m were taken over from the original turbine manufacturer's documentation. The force F_p was simulated by the forces in axial direction (the x axis direction) at the points of the shaft flange connection with the runner. The shaft's own weight was simulated by gravitational acceleration. The runner's weight was reduced to the points of connecting the flange with runner. The torque was simulated by the forces in radial direction in all the nodes at the shaft flange circumference, so that the total torsion moment from these forces represents the torque, while the bending moments of these forces as well as the forces themselves are mutually canceled.

3.3. Results of the numerical calculations

3.3.1. Load case 1

Fig. 15 shows the stresses, calculated by the finite elements method, at the location of crack initiation at the shaft flange, for the load case 1. Fig. 15a shows the stress contours of the normal tension stresses in the direction of the shaft axis σ_x, while Fig. 15b shows the equivalent stresses σ_{eqv} in the same zone, calculated according to the Von Mises's criterion. From the stress contours display maximum normal stress $\sigma_x = 119$ MPa and the maximum equivalent stress $\sigma_{eqv} = 127$ MPa can be read in the same node on the flange radius, which corresponds to the real location of cracks initiation, Figs. 2–4.

3.3.2. Load case 2

Fig. 16 shows the stresses, at the location of crack initiation at shaft flange, for the load case 2. Fig. 16a shows the stress contours of the normal tension stresses in the direction of shaft axis σ_x, while Fig. 16b shows equivalent stresses σ_{eqv} in the same zone, calculated according to the Von Mises' criterion. From the stress contours display the maximum normal stresses $\sigma_x = 47.8$ MPa, $\sigma_y = 12.5$ MPa and the maximum equivalent stress $\sigma_{eqv} = 57$ MPa can be read in the same node on the flange radius, which corresponds to the real crack initiation location, Figs. 2–4.

The change of the total normal stress $\sigma_n = \sqrt{\sigma_x^2 + \sigma_y^2}$ in the node of FEM mesh at the flange radius in which the maximum stresses occur (the equivalent and total normal load) is shown in Fig. 17 for one rotation of the shaft, i.e. one load change cycle. The maximum stress value σ (max) occurs when the monitoring node is on the top position during shaft rotation, and σ (min) occurs when the monitoring node is on the bottom position during shaft rotation. It can be seen from the diagram in Fig. 17 that the stress ratio is: $R = \sigma\ (\text{max})/\sigma\ (\text{min}) = -0.86$. Also, the average total normal stress value is calculated by expression: $\sigma_{sr} = (\sigma\ (\text{max}) + \sigma\ (\text{min}))/2$ and shown in Fig. 17.

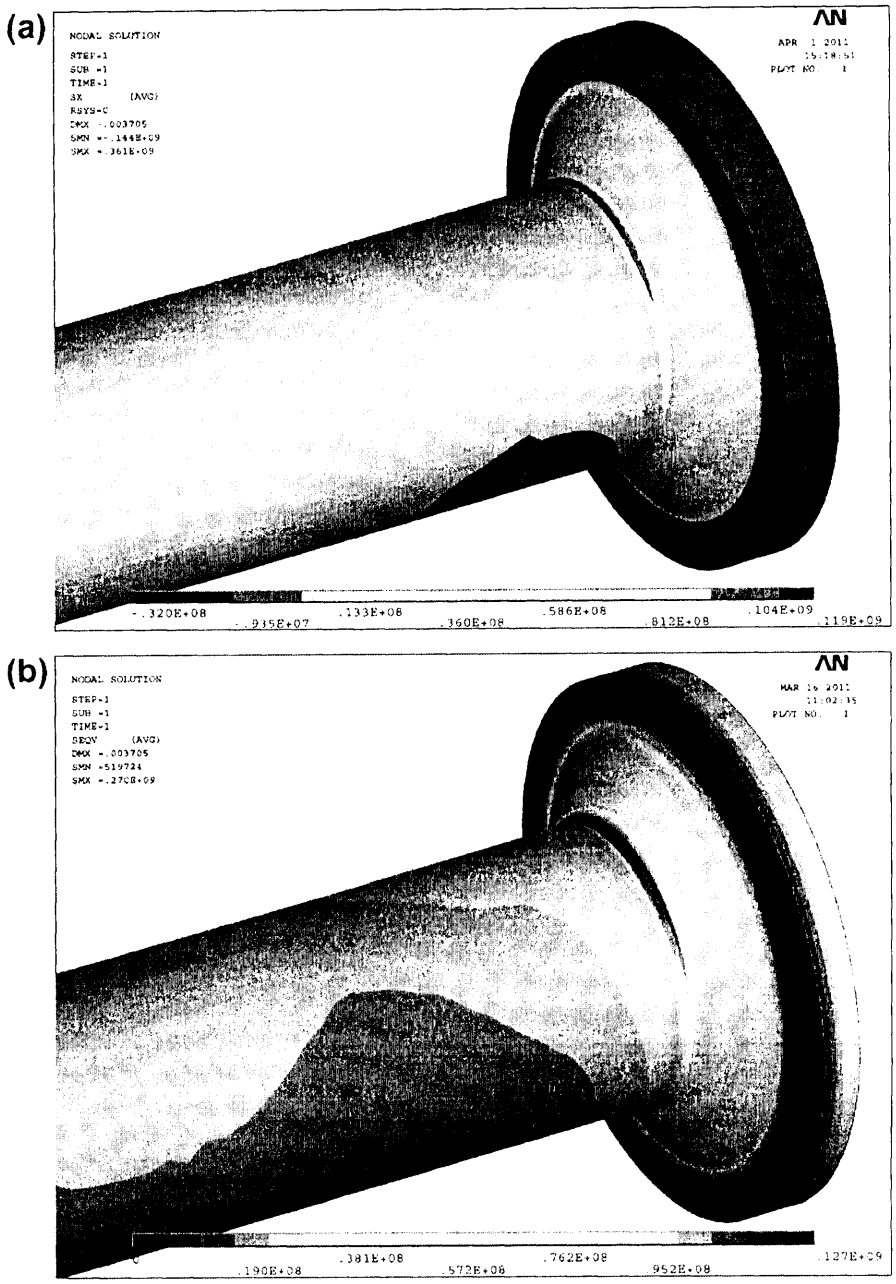

Fig. 15. Finite element analysis results for the load case 1, (Pa).

4. Discussion

The chemical composition of the tested shaft flange material corresponds to the requirements of the GOST 977-88 standard [6]. The fact that some of the obtained elongation values were lower than the minimal required, shows that there are locations in the microstructure that have reduced ability for plastic deformation. So, in these locations easier occurrence of initial cracks can be expected.

The established tensile properties, specifically tensile strength and elongation values, are lower than required ones, i.e. the tested steel casting sample does not fully meet the tensile characteristics requirements stated in the GOST 977-88 standard [6]. From the point of view of toughness, the presented and analyzed results of testing the notch impact strength shows that the material meet the requirements of the reference standard [6].

The results of micro-structural analysis in light microscope show that the microstructure was cast fine grained, ferrite-pearlite microstructure with non-metallic oxide-type inclusions and with sporadic dendrite-structure participation. The presence of microcracks is also noticed.

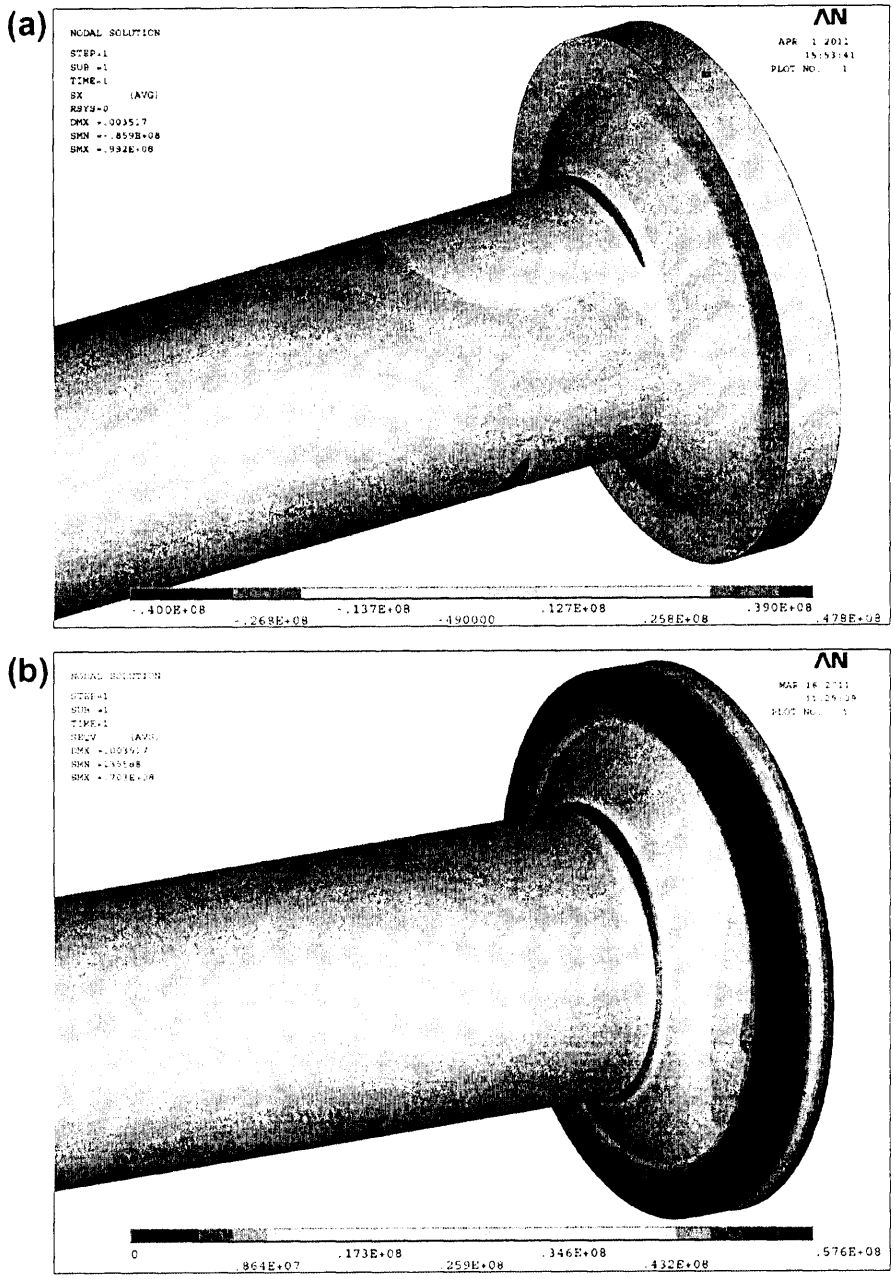

Fig. 16. Finite element analysis results for the load case 2, (Pa).

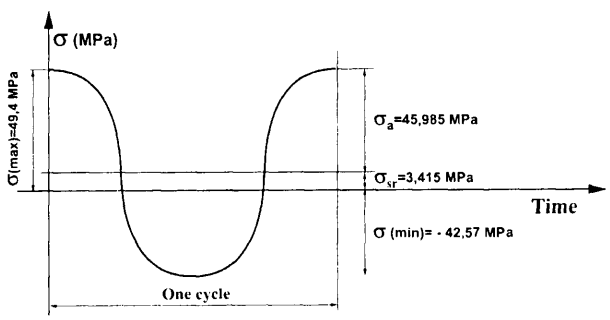

Fig. 17. Total normal stresses in the course of one revolution.

Fig. 18. Fine cracks in the critical zone of shaft-flange transition zone, found by magnetic particle testing after fine grinding.

According to the heat treatment regime stated by the shaft manufacturer, it could be expected that complete austenization was done, with breaking the dendrite microstructure that had remained from the casting process. However, the obtained microstructure test results, shown on Fig. 11, demonstrate that some portion of residual dendrite microstructure has remained. Such non-homogeneous microstructure, together with the observed porosity and microcracks, has contributed to faster propagation of the fatigue crack, compared with the case of the flange material that completely fulfill requirements [6].

According to [5], fatigue limit at $R = -1$ in open air is 225 MPa, and 140 MPa in water. However, by testing the flange material samples, the value of 168 MPa of fatigue limit in open air was obtained, which is ≈25% less than the reference value of 225 MPa.

It was determined by visual inspection that the anticorrosive coating was delaminated from the metal surface and that the zone of the shaft-flange transition radius was directly exposed to the effects of river water due to inadequate sealing of the shaft seal box.

In the same time when this failure analysis was conducted, the non-destructive testing of other turbine shafts of the same type revealed numerous cracks, Fig. 18. The cracks were found in zone of the same width as obtained by Finite element calculation, Fig. 16, for the load case 2. The pattern of the cracks at the metal surface and the presence of the one major crack accounting for failure indicate corrosion fatigue as the cause of the failure [12–14].

Numerical calculations show that the distribution of stresses and deformations in the shaft with flange was in accordance with the expected ones. Width of the maximum stress zone, obtained by the Finite element analysis, strongly correlates with the width of the zone determined by non-destructive inspection. The maximum normal stress in the critical point of the transient radius at static load, during start of operation and change of runner blades' position, is 119 MPa, which gives high safety factor in comparison with the obtained yield stress of 310 MPa. The obtained value for the normal tensile stress of 47.8 MPa during normal shaft operating regime is less than the test value of the fatigue limit of 168 MPa, so the cause of initial cracks occurrence cannot be found in the shaft properties. The level of normal stresses during start of operation (119 MPa) is approximately 75% of fatigue limit, which was insufficient safety margin for "wet" environment.

Also, the tensile stress values on the shaft-flange transition radius, obtained by the Finite element analysis, for the load case 2 (47.8 MPa) are higher than the recommended one (⩽40 MPa) for this type of shafts [15,16].

The calculated induced stress intensity factor (SIF) range at the crack tip was 13.1 $MPa\sqrt{m}$ and that is higher than the threshold SIF range for the material, 4.2 $MPa\sqrt{m}$, which explains the stable crack growth on the shaft during service [17].

On the basis of all the above stated, it can be concluded that corrosive fatigue was the cause of the shaft failure. The root cause of this turbine shaft failure can be found in the design of the seal box and insufficiently developed procedures for non-destructive periodical inspection and anticorrosion protection of the transition zone.

5. Conclusions

Despite the fact that 20GSL material has not fully fulfilled the requirements [6], the reasons for the premature failure cannot be completely attributed to the material quality.

The shaft failure occurred due to the combination of several factors:

- Inappropriate corrosion protection in the zone of critical radius and lack of procedures of renewing corrosion protection of turbine shaft.
- Corrosion, i.e. corrosion fatigue due to leakage of river water through the sealing box.
- High stresses during start/stop cycles and during regular operating regime in the zone of transition radius for "wet" environment.

The following suggestions emerged from this failure analysis:

- Redesign of the seal box in order to eliminate of water leakage into the shaft-flange transition zone.
- Redefining of procedures for periodical non-destructive inspection of the shaft-flange transition zone status, with increased frequency.
- Periodical renewal of the anticorrosive protection on the shaft flange, especially in the shaft-flange transition zone.
- Checking the possibility for redesign the transient radius for reducing the stress level at critical radius.
- Keeping the start/stop cycles at minimal values as it is possible.
- Considering an improvement of general technical conditions of delivery for flange material upon a new commissioning.

Acknowledgements

Parts of this research were supported by the Ministry of Sciences and Technology of Republic of Serbia Grant TR 35029 – Development of Methodology for Improvement of Operational Performance, Reliability and Energy Efficiency of Machine Systems used in the Resource Industry.

References

[1] Bachschmid N, Pennacchi P, Tanzi E. Cracked rotors – a survey on static and dynamic behavior including modelling and diagnosis. Heidelberg-Berlin: Springer; 2010.
[2] Braitsch W, Haas H. Turbines for hydroelectric power. In: Heinloth K, editor. Landolt-Börnstein, group VIII: advanced materials and technologies, vol. 3: energy technologies, subvol. C: renewable energies. Heidelberg-Berlin: Springer Verlag; 2006. p. 493–604.
[3] Arne Kjølle. Hydropower in Norway – mechanical equipment, survey, NTNU. Department of energy and process engineering. Trondheim; 2001.
[4] Egusquiza E, Valero C, Estévez A, Guardo A, Coussirat M. Failures due to ingested bodies in hydraulic turbines. Eng Fail Anal 2011;18:464–73.
[5] Bulloch JH, Callagy AG. An detailed integrity assessment of a 25 MW hydro-electric power station penstock. Eng Fail Anal 2010;17:387–93.
[6] GOST 977-88, Steel Catings. General Specification; 1988.
[7] Wulpi DJ. Failures of shafts, in ASM handbook. Failure analysis and prevention, vol 11. ASM International; 2002.
[8] GOST 1497-84, Metals. Methods of tension test; 1984.
[9] GOST 9454-78, Metals. Method for testing the impact strength at low, room and high temperature; 1978.
[10] GOST 25.502-79 – Strength analysis and testing in machine building. Methods of metals mechanical testing. Methods of fatigue testing; 1979.
[11] Troschenko VT. Fatigue resistance of metals and alloys. Naukova Dumka; 1987. p. 668–70. [in Russian].
[12] Winston Revie R, Uhlig Herbert H. Corrosion and corrosion control. John Wiley & Sons, Inc; 2008.
[13] Gangloff RP. Corrosion fatigue cracking, in corrosion tests and standards: application and interpretation. In: Baboian R, editor. ASM International; 2005. p. 302–21 [2nd ed.].
[14] Ebara R. Corrosion fatigue phenomena learned from failure analysis. Eng Fail Anal 2006;13:516–25.
[15] Maricic T, Haber D, Pejovic S. Standardization as prevention of fatigue cracking of hydraulic turbine-generator shaft. In: Proceedings of IEEE electrical power conference on CD. Montreal; 2007.
[16] Atanasovska, Mitrović R, Momčilović D. FEM model for calculation of hydro turbine shaft. In: Proceedings – the sixth international symposium KOD 2010, 29–30.09.2010. Palić, Serbia, Published by Faculty of Technical Science – Novi Sad, Serbia; 2010. p. 183–8.
[17] Döker H. Fatigue crack growth threshold: implications, determination and data evaluation. Int J Fatigue 1997;19(1):S145–9.

Database of Steel and Alloy (Marochnik)

Characteristics for grade 20GSL (20ГСЛ)

Grade :	20GSL (20ГСЛ)
Classification :	Casting alloy steel for general purposes
Equivalent grades:	Go here

Chemical composition in % for grade 20GSL (20ГСЛ)

C	Si	Mn	S	P
0.16 - 0.22	0.6 - 0.8	1 - 1.3	max 0.03	max 0.03

Mechanical properties under T=20°C for grade 20GSL (20ГСЛ)

Assortment	Dimension	Direct.	s_B	s_T	d_5	y	KCU	Heat treatment
-	mm	-	MPa	MPa	%	%	kJ / m^2	-
Casting heat-treatment, GOST 977-88			540	294	18	30	294	Normalizing and drawing

Heat treatment of the material 20GSL (20ГСЛ)

Normalizing 870 - 890 ° C, Tempering 570 - 600 ° C

Equivalent steels for grade 20GSL (20ГСЛ)

Warning! Indicated both exact and nearest equivalents.

USA	Germany	Japan	France	England	European	Italy	Spain	China	Sweden	Hungary	Czechia	Australia	Switzerland	South Korea
-	DIN,WNr	JIS	AFNOR	BS	EN	UNI	UNE	GB	SS	MSZ	CSN	AS	SNV	KS
1022 1518 G10220 G15180 G15220 H15220	1.1133 20Mn5 G21Mn5 GS-20Mn5	SMnC420	20M5	120M19 20Mn5	1.1133 20Mn5	20Mn7 G22Mn3	20Mn6 F.1515 F.220A	20MnG	2132	Ao20Mn5	422714	1022	20Mn5	SMnC420

Specification :

Mechanical properties :

s_B - Tensile strength , [MPa]

s_T - Yield stress, [MPa]

d_5 - Specific elongation at fracture , [%]

y - Reduction of area , [%]

KCU - Impact strength , [kJ / m^2]

HB - Brinell hardness , [MPa]

20GSL (20ГСЛ) - Casting alloy steel for general purposes: chemical composition, mechanical and physical properties, hardness
Database of steels and alloys (Marochnik) contains information about chemical composition and properties more then 3000 steels and alloys